AGU100 ADVANCING EARTH AND SPACE SCIENCE

Geophysical Research Letters

RESEARCH LETTER

10.1029/2018GL078822

Key Points:

- The high occurrence rate of postmidnight ESF during solstices of the 2008–2009 solar minimum is examined
- Postmidnight June solstice ESF are shown to have been originated, predominantly, in the midnight to postmidnight sector
- During December solstice, ESF events and conditions for their development start in the evening sector and extend through midnight

Correspondence to:
W. Zhan,
Weijia.Zhan@utdallas.edu

Citation:
Zhan, W., Rodrigues, F., & Milla, M. (2018). On the genesis of postmidnight equatorial spread *F*: Results for the American/Peruvian sector. *Geophysical Research Letters*, *45*, 7354–7361. https://doi.org/10.1029/2018GL078822

Received 18 MAY 2018
Accepted 9 JUL 2018
Accepted article online 16 JUL 2018
Published online 14 AUG 2018

On the Genesis of Postmidnight Equatorial Spread *F*: Results for the American/Peruvian Sector

Weijia Zhan[1], **Fabiano S. Rodrigues**[1], and **Marco A. Milla**[2]

[1]W. B. Hanson Center for Space Sciences, The University of Texas at Dallas, Richardson, TX, USA, [2]Jicamarca Radio Observatory, Lima, Peru

Abstract Previous studies of the Earth's low-latitude ionosphere using in situ measurements made by sensors on the Communication/Navigation Outage Forecasting System (C/NOFS) satellite showed an unexpected predominance of equatorial spread *F* (ESF) events in the postmidnight sector during June and December solstice months of the 2008–2009 deep solar minimum. It has been suggested that these events might have been driven by the unusual behavior of the equatorial plasma drifts, which showed an abnormal upward peak around midnight during the same period. We use coherent backscatter radar (Jicamarca Unattended Long-term Investigations of the Ionosphere and Atmosphere - JULIA) measurements made at the Jicamarca Radio Observatory (11.95°S, 76.87°W, ∼ 1° dip lat) in Peru to better understand the origin of the ESF irregularities observed by C/NOFS. The radar observations show that ESF events during December solstice start in the postsunset sector. These ESF events and the conditions for their development are shown to continue through midnight hours. The predominance of postmidnight irregularities on C/NOFS observations during December solstice is caused by the slow vertical development of the ESF structures, which only reach the topside near midnight in most cases. On June solstice, however, JULIA observations show that ESF started predominately in the midnight to postmidnight sector. Collocated digisonde observations provide additional insight on *F*-region conditions leading to these ESF events.

Plain Language Summary Equatorial spread F (ESF) is the name given to a broad spectrum of irregularities in the low-latitude ionospheric electron density. ESF irregularities affect the propagation of radio signals used in various applications (remote sensing, navigation, communications, etc.). In this study, we analyzed radar observations of the evolution (in time and height) of ESF events made at the Jicamarca Radio Observatory, in Peru. The analysis was performed to better understand the morphology and the origin (in LT) of postmidnight ESF observed by satellites during the extreme solar minimum of 2008/2009. Our results show that, for the Peruvian sector, June solstice postmidnight ESF events started predominately in the postmidnight sector. December solstice ESF events and conditions for their evolution, however, started in the postsunset sector and continued to exist until postmidnight hours.

1. Introduction

Equatorial spread *F* (ESF) is the name given to signatures of ionospheric irregularities observed at equatorial and low-latitudes by a variety of space- and ground-based instruments (e.g., Abdu et al., 1981; Kelley et al., 1976; McClure et al., 1977; Sobral et al., 1980; Woodman & La Hoz, 1976). The development of ESF irregularities is commonly explained by the Generalized Rayleigh-Taylor instability (Sultan, 1996). The main factor controlling the conditions for Generalized Rayleigh-Taylor instability growth is often credited to the upward component of the $\mathbf{E} \times \mathbf{B}$ drifts (e.g., Fejer et al., 1999). A prereversal enhancement (PRE) of the upward drifts (Eccles et al., 2015) is observed around sunset hours in most longitude sectors during equinoctial months (e.g., Gentile et al., 2006) and explains, for the most part, the high occurrence rate of ESF events observed in the postsunset sector (e.g., Fejer et al., 1999; Smith et al., 2016).

The Communication/Navigation Outage Forecasting System (C/NOFS) satellite was launched in 2008 with the main objective of studying ESF and the effects of these events on radio propagation and applications (de La Beaujardiere, 2004). C/NOFS was launched on a low inclination (13°) elliptical orbit, with an orbital period of ∼97 min. The orbit had a perigee of 405 km and an apogee of 853 km at the beginning of the mission. The satellite reentered the Earth's atmosphere on 28 November 2015 after about 7.5 years of nearly uninterrupted observations. One of the first and most interesting findings of the C/NOFS mission is an unexpected behavior in the occurrence of ESF (e.g., Burke et al., 2009; Heelis et al., 2010; Su et al., 2009; Yizengaw et al., 2013).

Heelis et al. (2010), in particular, analyzed ion density perturbations based on measurements made in the deep solar minimum of 2008–2009 by sensors that are part of the Coupled Ion Neutral Dynamics Investigation (CINDI) instrument package on C/NOFS. They pointed out a maximum in the occurrence rate of irregularities across midnight into the postmidnight hours during June and December solstices. This behavior greatly departed from expectations based on previous observations.

Stoneback et al. (2011) then analyzed low-latitude drift measurements made between 2009 and 2010 by the ion velocity meter sensor on CINDI. They found a semidiurnal component in the variation of the vertical component of the equatorial plasma drifts. While the semidiurnal variation was observed in all seasons, it was strongest in June and December solstices. This semidiurnal variation led to downward drifts in the afternoon and upward drifts around midnight. Stoneback et al. (2011) pointed out that the upward drifts near midnight correspond to the regions with a high occurrence rate of postmidnight irregularities, which indicates a potential causal relationship between the observed drifts and ESF.

Here we take advantage of the long-term observations of equatorial *F*-region irregularities made by the 50 MHz coherent backscatter radar (Jicamarca Unattended Long-term Investigations of the Ionosphere and Atmosphere, JULIA; Hysell & Burcham, 1998) of the Jicamarca Radio Observatory to study the response of ESF occurrence to changes in solar flux conditions, including those of the deep solar minimum in 2008–2009 in the American sector. Using these measurements, we produce maps (height versus local time) of irregularity occurrence for different seasons and solar flux conditions between 1996 and 2015. We then use these maps to better understand the genesis, development, and decay of ESF irregularities in the American sector under different seasonal and solar activity conditions. We seek, in particular, to use ground-based observations to better understand the origin, in local time, of postmidnight ESF events detected by previous satellite (topside) observations during the 2008–2009 solar minimum.

2. Measurements and Analyses

2.1. Measurements

The JULIA radar is a 50-MHz coherent backscatter radar system that is part of a set of ground-based instruments located at the Jicamarca Radio Observatory (11.95°S, 76.87°W, ~ 1° dip lat; Hysell & Burcham, 1998). In the initial implementation of JULIA, two 30-kW transmitters were used to excite the north and south quarters of the Jicamarca antenna. These transmitters were combined as to maximize the directivity of the combined pattern in the direction perpendicular to the geomagnetic field at *F*-region heights. This maximizes the sensitivity of the system to field-aligned irregularities. Receivers were also connected to the east and west quarters of the Jicamarca antenna. This setup allowed interferometric analyses of the echoes and the determination of the zonal component of irregularity velocity.

While modifications to JULIA have been made since its first light in 1996, the system continued to be able to make routine (150–200 days/year) coherent backscatter radar observations of daytime and nighttime echoes caused by field-aligned ionospheric irregularities at E- and F-region heights. The measurements used in this study consist of the signal-to-noise ratio (SNR) of the nighttime *F*-region echoes observed by JULIA. For nighttime *F*-region observations, the measurements typically start 18:00 LT and end at around 08:00 LT the next day. The measurements made by JULIA cover altitudes ranging from about 90 to 800 km or above.

Figure 1a shows the Range-Time-Intensity (RTI) map of the JULIA measurements made on 2 March 2000. The RTI map shows a typical example of an ESF event detected by JULIA. It shows the appearance of the first echoes around 19:30 LT coming from a bottom-type layer located around 350 km altitude. The bottom-type is then followed by the appearance of topside echoing layers (plumes) starting at 20:00 LT. By 23:00 LT, very few echoes are detected by JULIA. Departures from this pattern driven by solar flux conditions are addressed in this study.

2.2. Analyses

In order to better understand the response in the genesis, development, and decay of irregularities to solar flux conditions, we analyzed the RTI maps of JULIA measurements made between 1996 and 2015. Measurements made on 2,470 days during that period were available and used in this study.

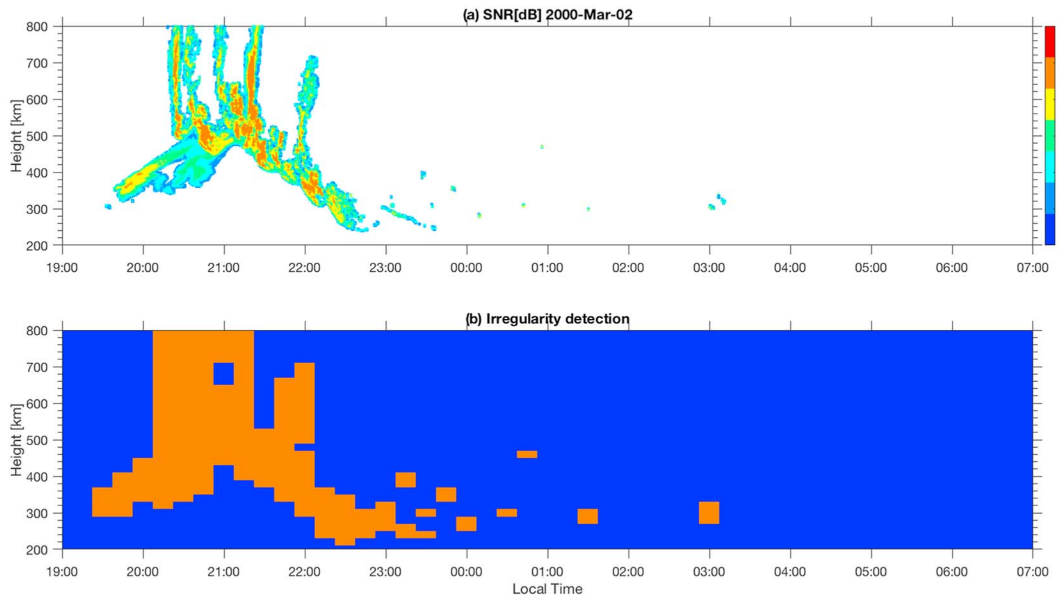

Figure 1. (a) Shows an example of the Range-Time-Intensity map of echoes measured by JULIA on 2 March 2000. (b) Shows the regions where equatorial spread *F* irregularities were identified based on number of echoes above a certain SNR threshold. Please, see text for more details. SNR = signal-to-noise ratio.

In order to obtain information about the morphology of ESF over Jicamarca, we created maps of the seasonal occurrence rate of irregularities for each year between (and including) 1996 and 2015. To create these maps, we carefully analyzed each JULIA RTI map and determined the occurrence of irregularities as a function of height and LT. Figure 1 illustrates the process. Figure 1a shows an example of the RTI SNR values available for this study. Figure 1b shows the locations (in height and time) for which measurements were available (blue or orange regions) and the locations where irregularities were identified (orange regions). The irregularities were identified based on number of echoes above a certain SNR within a time versus height interval. The observations for each day were grouped in a height versus time matrix. The matrix has resolutions of 15 min and 20 km in height. Irregularity detection is assigned to a matrix bin when more than 10 echoes with SNR greater than −20 dB were detected. The SNR threshold (−20 dB) and number of echoes (at least 10) were chosen as to minimize the misidentification of interference and clutter as echoes caused by ESF irregularities. Despite our efforts, we were still forced to remove a number of measurements from our analyses due to strong contamination of the observations by interference from artificial sources. As a result, we were left with 2,457 days of observations for our analyses.

We also only considered measurements made during geomagnetically quiet conditions. Each SNR value was tagged with the geomagnetic Planetary K (Kp) index value at the time of the measurement and the previous four Kp values. Only observations with all the five Kp values less than 4 were considered in our analysis.

The observations available for this study cover a broad range of solar flux conditions, which can be represented by the F10.7 solar flux index. The variation of F10.7 index over the observation period (1996 to 2015) is shown in Figure 2. It covers two solar maxima and two minima including the extreme solar minimum of 2008–2009.

3. Results and Discussion

Figure 3 summarizes the results of our analyses. It shows the response of the seasonal occurrence of radar ESF to varying solar flux conditions. The left panel shows the variation of the average solar flux index for each season from 1996 to 2015. The other panels show the occurrence rates of ESF irregularities observed by JULIA for each season from 1996 to 2015. The occurrence rates correspond to number of days where ESF was detected over the total number of observation days. Seasons were also organized based on ±45 days centered around 21 March (March Equinox), 21 June (June solstice), 21 September (September Equinox), and 21 December (December solstice). White regions in the panels indicate times when less than 10 observation days are available.

10.1029/2018GL078822

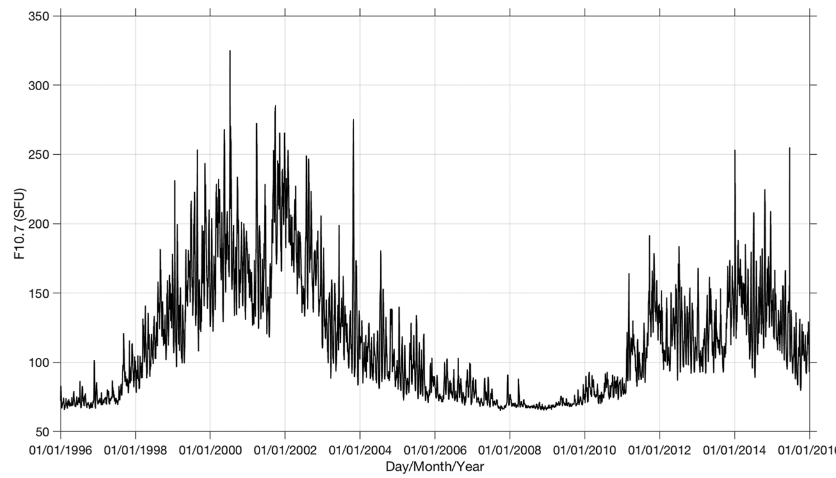

Figure 2. Variation of the solar flux index (F10.7) during the period under which JULIA measurements were made.

3.1. On Post-Sunset ESF

As expected, our results show a strong seasonal variation in the occurrence rates of postsunset ESF. ESF is observed to occur, predominantly, during equinox and December solstice when the PRE is well developed (Fejer et al., 1999; Smith et al., 2016). During June solstice, however, ESF occurrence rates are severely reduced.

Our results also show that postsunset ESF starts to be observed at earlier local times during periods of high solar activity, which is in agreement with previous studies (e.g., Chapagain et al., 2009; Cueva et al., 2003; Fejer et al., 1999; Hysell & Burcham, 1999; Smith et al., 2016). Also in agreement with previous studies is the appearance of the first echoes at higher altitudes during periods of high solar activity. Finally, we also found

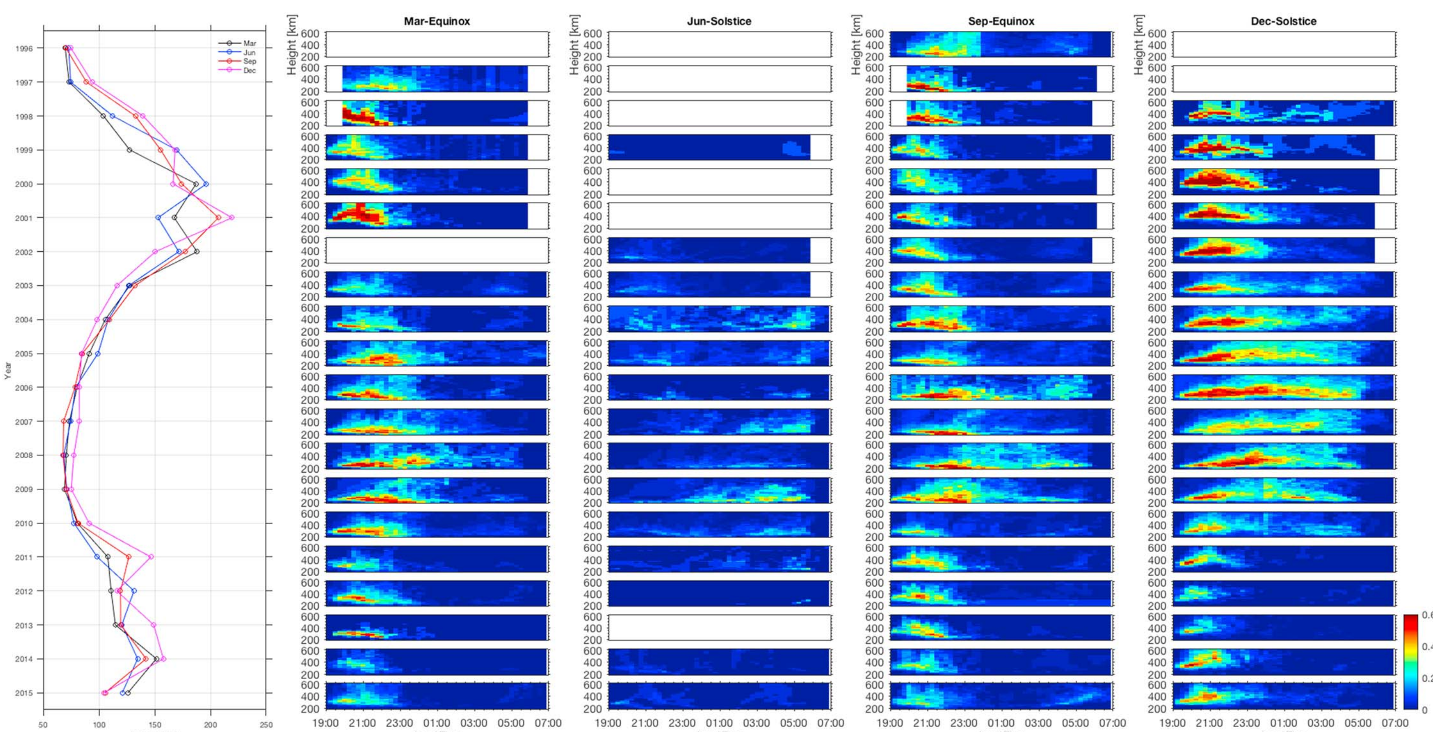

Figure 3. Occurrence rates of quiet time equatorial spread *F* observed by JULIA between 1996 and 2015. Only seasons with at least 10 days of observations are shown. The left panel shows the variation of the average F10.7 index for each year. Curves are shown the four different seasons: March Equinox, June solstice, September Equinox, and December solstice. The top panels show height versus local time maps of the seasonal occurrence rates of equatorial spread *F* for each year. sfu = solar flux unit.

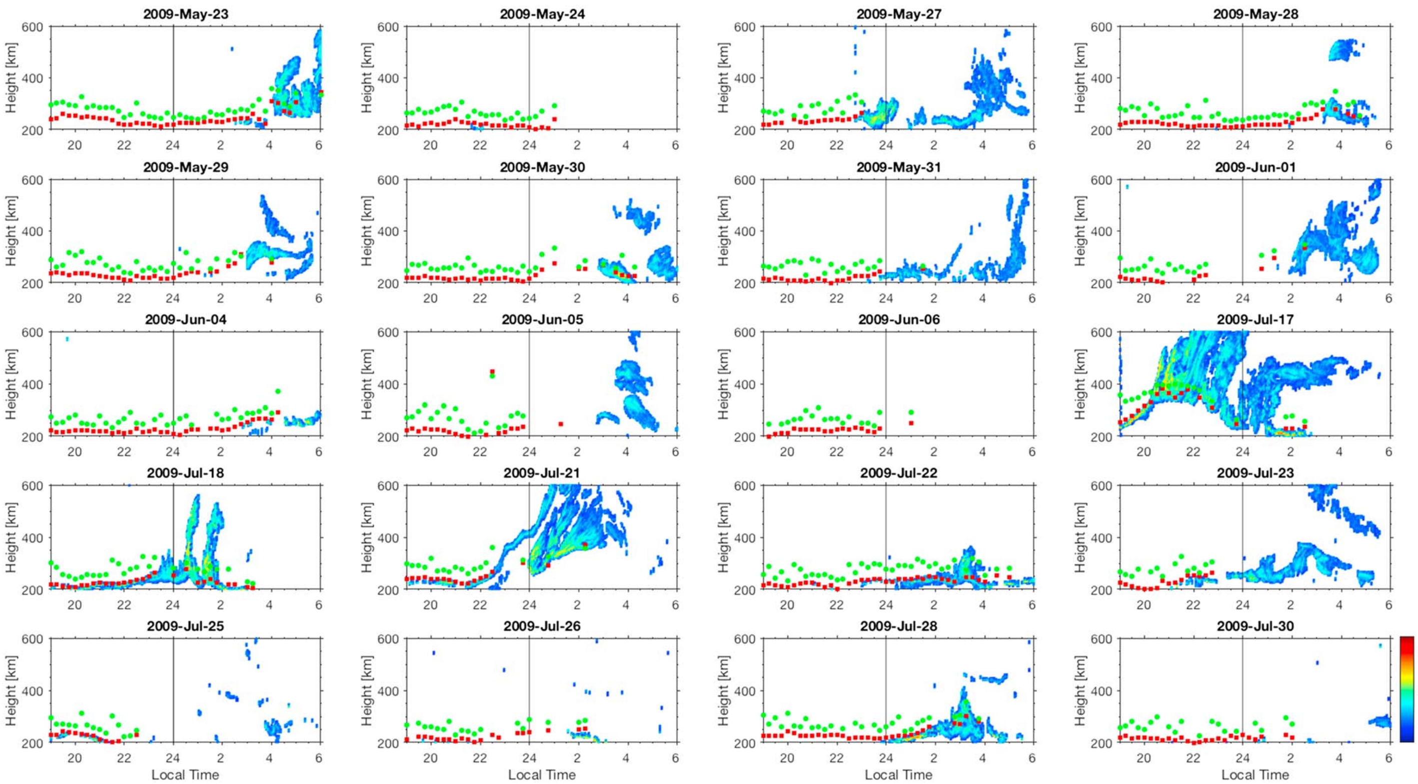

Figure 4. Examples of JULIA Range-Time-Intensity maps for June solstice 2009. Each panel also shows the variation of h′F (red markers) and hmF2 (green markers) measured by a collocated digisonde.

that during periods of high solar activity, the echoes reach a threshold altitude (say, 400 km) more quickly than during periods of low solar flux activity.

Our results also show that postsunset echoes last longer during periods of low solar flux conditions. This is credited to weaker downward drifts (stabilization) after the PRE during periods of low solar activity (Fejer et al., 1999; Hysell & Burcham, 1999; Smith et al., 2016). This effect is more pronounced during December solstice but is also observed during equinox. During equinoctial months, significant occurrence rates (say >50%) are observed until about 22:00 LT under moderate to high solar flux conditions and until midnight during periods of low solar flux. During December solstice, however, significant occurrence rates can be observed until dawn (00:50–06:00 LT) under low solar flux conditions.

Unfortunately, there is a gap in the JULIA observations of June solstice ESF for periods of high solar flux conditions (years 1996–1998, 2000, and 2001). The June solstice measurements available for this study were mostly made under low or moderate solar flux activity (average F10.7 <130 solar flux unit). While the observations do not allow us to identify an obvious pattern for June solstice, it suggests a reduction in postsunset events during low solar flux conditions (See years 2007–2010).

3.2. On Postmidnight ESF

Of main interest to this study is the occurrence of postmidnight ESF events and the response to seasonal and solar flux variations. As mentioned earlier, C/NOFS found a predominance of ESF occurrence rates in the postmidnight sector during June and December solstices of the 2008–2009 deep solar minimum, which were linked to unusual upward drifts observed around midnight (Heelis et al., 2010; Stoneback et al., 2011).

The results of our analysis (Figure 3) indeed show high occurrence rates of ESF in the postmidnight sector during June solstice 2009. The results also show high occurrence rates of ESF during postmidnight hours in December solstice 2009. This is in agreement with C/NOFS satellite observations. The height versus local time maps of ESF occurrence created with JULIA measurements, however, provide additional insights on the origin in local time of postmidnight ESF. During June solstice, the ESF occurrence rates during premidnight hours

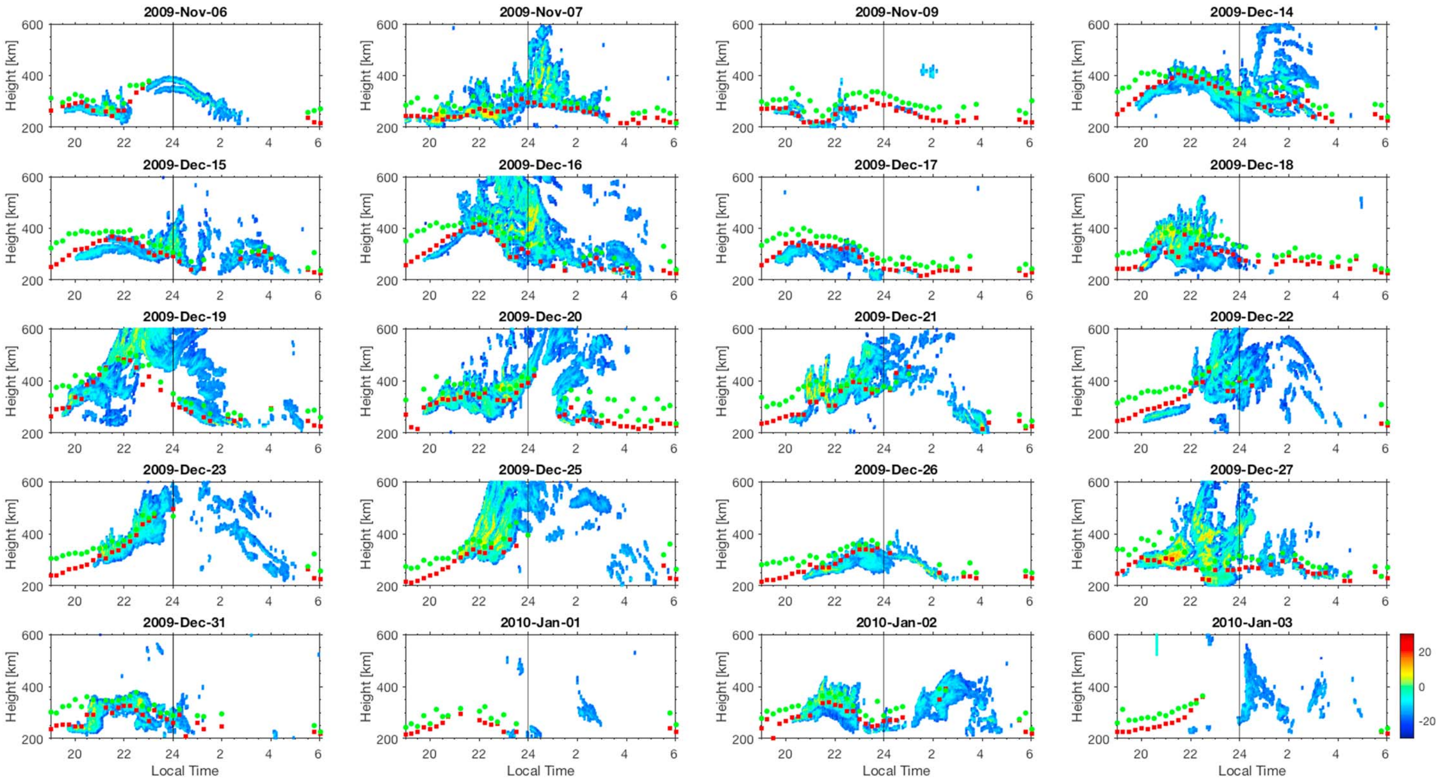

Figure 5. Examples of JULIA Range-Time-Intensity maps for December solstice 2009. Each panel also shows the variation of h′F (red markers) and hmF2 (green markers) measured by a collocated digisonde.

were negligible. This indicates that ESF observed by C/NOFS in the American (Peruvian) sector would not have originated in the postsunset sector near Jicamarca.

In order to provide more information about the ESF events observed by JULIA during June solstice 2009, we show 20 RTI maps of full-night observations made during that period in Figure 4. Along with the RTI maps, we also provide variations in the height of the *F*-region peak (hmF2) and in the virtual height of the *F*-region base (h′F) as measured by a collocated digisonde.

The radar observations in Figure 4 serve to illustrate and confirm that the overwhelming majority of ESF events were first detected in the postmidnight sector. Only one postsunset ESF event (on 17 July) was observed during June solstice 2009. Most of the postmidnight events were observed well after midnight (after 02:00 LT) and could have been the product of upward drifts around midnight as hypothesized by Stoneback et al. (2011). This is also in agreement with the results of Yizengaw et al. (2013). They used vertical drifts measured by C/NOFS and an assimilative physics-based model of the low-latitude ionosphere (Retterer et al., 2005) to show that the *F*-region can become unstable in the postmidnight sector during June solstice low solar flux conditions.

On the other hand, one could propose that the observed ESF events could have been generated at an evening sector to the west of the radar site. Under typical ionospheric convection conditions, ESF would then drift to east for several hours where it would be detected by JULIA in the postmidnight sector. Assuming development at around 20:00 LT, observation by JULIA at 02:00 LT and an average zonal plasma drift of 75 m/s, the ESF event would have been originated $\sim$ 15° in longitude to the west of Jicamarca.

To better understand the underlying *F*-region behavior over Jicamarca and potential conditions leading to ESF generation, we also investigated temporal variations in the h′F and hmF2 parameters measured by the Jicamarca digisonde. The digisonde parameters are also shown in Figure 4. These parameters do indicate that the layer is lifted, though modestly, prior to the appearance of ESF in most days. The RTI maps for 23 May and 18 and 28 July show, perhaps, some of the most clear examples of the apparent *F*-region uplifts prior to ESF development during geomagnetically quiet conditions. The uplift associated with the severe ESF event of 21

July occurred during geomagnetically disturbed conditions. The observations indicate that under extreme conditions of atmospheric contraction of the 2008–2009 solar minimum, apparent uplifts could have led to destabilization of the *F*-region layer and ESF generation.

Therefore, the RTI maps in Figure 4 reinforce our inference from the climatology in Figure 3, that is, a predominant occurrence of postmidnight ESF events in June solstice 2009. More importantly, the RTI maps also indicate that the ESF events over Jicamarca were not generated during postsunset hours in that longitude sector. Collocated digisonde observations provide additional evidence that the postmidnight events were associated with apparent *F*-region uplifts. Unfortunately, the measurements available do not allow us to determine the source of the observed uplifts. Some of the observed uplifts could result from the unusual, quiet time midnight vertical drifts measured by C/NOFS during the 2008–2009 solar minimum driven, presumably, by semidiurnal tides. Yizengaw et al. (2013) could be driven by atmospheric gravity waves, traveling ionospheric disturbances, and by electric fields associated with off-equatorial sporadic-E layers. It is also possible that the apparent uplifts are a result of weakening downward drifts as proposed by Nicolls et al. (2006) and recently investigated by Ajith et al. (2016) and Zhan and Rodrigues (2018) with measurements and modeling parameters for the Indonesian and American sector, respectively.

We now turn our attention to observations made during December solstice under the extreme low solar flux conditions. Figure 5 shows 20 RTI maps of full-night observations during December solstice 2009. Again, we also show the variations in h'F and hmF2 measured by the Jicamarca digisonde. As indicated by the climatological results of Figure 3, an overwhelming number of ESF events during that period start during postsunset hours. ESF behavior in December follows the expected pattern for typical ESF events. The events start in the postsunset sector as bottom-type or bottomside layers, and then give place to fully developed (topside) layers later on. The ESF events slowly gain altitude and reach LEO altitudes (say 400 km) typically after 22:00 LT.

Unlike June solstice, the layer starts to rise around 19:00 LT. In several cases, h'F and hmF2 reach their maximum excursion between 21:00 and 23:00 LT as a result of the expected variation in the vertical plasma drifts (PRE). The rise of the layer destabilizes the *F*-region producing postsunset ESF. In a few other cases, however, the layer is observed to rise until midnight. This midnight rise can be more clearly seen on 21, 22, 23, and 25 December. During those days, we hypothesize that the increases in *F*-region height could be the manifestation of the midnight upward drifts observed by C/NOFS. They would provide favorable conditions (elevated *F* layer) for ESF development throughout midnight.

More importantly, the RTI maps in Figure 5 serve to confirm our initial inference (from Figure 3) that December solstice ESF events start in the postsunset sector but most of them only reach the topside (or satellite altitudes) around midnight.

4. Conclusions

We used coherent backscatter radar (JULIA) measurements made at the Jicamarca Radio Observatory (11.95°S, 76.87°W, ∼ 1° dip lat) to better understand the origin, in local time, of irregularities observed by C/NOFS. We produce height versus local time maps of the occurrence rates of ESF as a function of season for each year between 1996 and 2015. These maps quantify the seasonal variability of ESF and the response of ESF morphology to solar flux conditions.

Of particular importance to this study is a better understanding of ESF occurrence and development during the deep solar minimum of 2008–2009, when sensors on the C/NOFS satellite showed an unexpected predominance of ESF events in the postmidnight sector (Heelis et al., 2010). It has been suggested that these events might have been driven by the unusual behavior of the equatorial plasma drifts, which showed an abnormal upward peak around midnight during the same period (Stoneback et al., 2011).

JULIA observations for June solstice 2009 showed an overwhelming dominance of ESF events that started around midnight or later. Collocated digisonde measurements confirm the absence of favorable conditions for postsunset ESF development during that period near the Jicamarca site (American Peruvian sector). More importantly, the digisonde observations showed apparent *F*-region uplifts preceding the appearance of postmidnight ESF structures. We hypothesize that these uplifts contribute to destabilization of the *F*-region and generation of postmidnight ESF. The set of observations available for this study does not allow us to determine the exact source (or sources) of the apparent uplifts.

JULIA observations for December solstice 2009, on the other hand, showed that ESF events and conditions for their development started in the postsunset sector and continued through midnight. Digisonde observations indicate the contributions of the well-known PRE and, in at least some cases, of apparent uplifts that continued until midnight. We interpret these uplifts as signatures of the abnormal drifts detected by C/NOFS.

The increased occurrence rate of postmidnight ESF seen by C/NOFS can be explained by the height coverage of the satellite. In general, ESF structures only reached the topside (and satellite altitudes) after 22:00 LT (Figure 5), and showed significant occurrence rates around midnight (Figure 3).

Acknowledgments
The radar measurements used in this study can be obtained from the Madrigal database (http://jro.igp.gob.pe/madrigal/). The Jicamarca Radio Observatory is a facility of the Instituto Geofisico del Peru operated with support from the NSFAGS-1433968 through Cornell University. FSR and WZ would like to thank support from AFOSR (FA9550-13-1-0095) and NSF (AGS-1554926). We would like to also thank Dr. Rod Heelis (UT Dallas) for helpful discussions.

References

Abdu, M. A., Batista, I. S., & Bittencourt, J. A. (1981). Some characteristics of spread F at the magnetic equatorial station Fortaleza. *Journal of Geophysical Research*, *86*(A8), 6836–6842. https://doi.org/10.1029/JA086iA08p06836

Ajith, K. K., Tulasi Ram, S., Yamamoto, M., Otsuka, Y., & Niranjan, K. (2016). On the fresh development of equatorial plasma bubbles around the midnight hours of June solstice. *Journal of Geophysical Research: Space Physics*, *121*, 9051–9062. https://doi.org/10.1002/2016JA023024

Burke, W. J., de La Beaujardiere, O., Gentile, L. C., Hunton, D. E., Pfaff, R. F., Roddy, P. A., et al. (2009). C/NOFS observations of plasma density and electric field irregularities at post-midnight local times. *Geophysical Research Letters*, *36*, L00C09. https://doi.org/10.1029/2009GL038879

Chapagain, N. P., Fejer, B. G., & Chau, J. L. (2009). Climatology of postsunset equatorial spread *F* over Jicamarca. *Journal of Geophysical Research*, *114*, A07307. https://doi.org/10.1029/2008JA013911

Cueva, R. Y. C., de Paula, E. R., & Kherani, A. E. (2003). Statistical analysis of radar observed *F* region irregularities from three longitudinal sectors. *Annales de Geophysique*, *31*, 2137–2146. https://doi.org/10.5194/angeo-31-2137-2013

de La Beaujardiere, O. (2004). C/NOFS: A mission to forecast scintillations. *Journal of Atmospheric and Solar - Terrestrial Physics*, *66*, 1573–1571. https://doi.org/10.1016/j.jastp.2004.07.030

Eccles, J. V., Maurice, J. P. S. t., & Schunk, R. W. (2015). Mechanisms underlying the prereversal enhancement of the vertical plasma drift in the low-latitude ionosphere. *Journal of Geophysical Research: Space Physics*, *120*, 4950–4970. https://doi.org/10.1002/2014JA020664

Fejer, B. G., Scherliess, L., & dePaula, E. R. (1999). Effects of the vertical plasma drift velocity on the generation and evolution of equatorial spread F. *Journal of Geophysical Research*, *104*(A9), 19,859–19,869. https://doi.org/10.1029/1999JA900271

Gentile, L. C., Burke, W. J., & Rich, F. J. (2006). A climatology of equatorial plasma bubbles from DMSP 1989-2004. *Radio Science*, *41*, RS5S21. https://doi.org/10.1029/2005RS003340

Heelis, R. A., Stoneback, R., Earle, G. D., Haaser, R. A., & Abdu, M. A. (2010). Medium-scale equatorial plasma irregularities observed by coupled ion-neutral dynamics investigation sensors aboard the communication navigation outage forecast system in a prolonged solar minimum. *Journal of Geophysical Research*, *115*, A10321. https://doi.org/10.1029/2010JA015596

Huang, C., & Hairston, M. R. (2015). The postsunset vertical plasma drift and its effects on the generation of equatorial plasma bubbles observed by the c/NOFS satellite. *Journal of Geophysical Research: Space Physics*, *120*, 2263–2275. https://doi.org/10.1002/2014JA020735

Hysell, D. L., & Burcham, J. D. (1998). JULIA radar studies of equatorial spread F. *Journal of Geophysical Research*, *103*(A12), 29,155–29,167. https://doi.org/10.1029/98JA02655

Hysell, D. L., & Burcham, J. D. (1999). Long term studies of equatorial spread F using the JULIA radar at Jicamarca. *Journal of Atmospheric and Solar-Terrestrial Physics*, *64*(12-14), 1531–1543. https://doi.org/10.1016/S1364-6826(02)00091-3

Kelley, M. C., Haerendel, G., Kappler, H., Valenzuela, A., Balsley, B. B., Carter, D. A., et al. (1976). Evidence for a Rayleigh-Taylor type instability and upwelling of depleted density regions during equatorial spread F. *Geophysical Research Letters*, *3*, 448–450. https://doi.org/10.1029/GL003i008p00448

McClure, J. P., Hanson, W. B., & Hoffman, J. H. (1977). Plasma bubbles and irregularities in the equatorial ionosphere. *Journal of Geophysical Research*, *82*(19), 2650–2656. https://doi.org/10.1029/JA082i019p02650

Nicolls, M. J., Kelley, M. C., Vlasov, M. N., Sahai, Y., Chau, J. L., Hysell, D. L., et al. (2006). Observations and modeling of post-midnight uplifts near the magnetic equator. *Annales de Geophysique*, *24*, 1317–1331. https://doi.org/10.5194/angeo-24-1317-2006

Retterer, J. M., Decker, D. T., Daniell, Jr. W. S. BorerR. E., & Fejer, B. G. (2005). Assimilative modeling of the equatorial ionosphere for scintillation forecasting: Modeling with vertical drifts. *Journal of Geophysical Research*, *110*, A11307. https://doi.org/10.1029/2002JA009613

Smith, J. M., Rodrigues, F. S., Fejer, B. G., & Milla, M. A. (2016). Coherent and incoherent scatter radar study of the climatology and day-to-day variability of mean F region vertical drifts and equatorial spread F. *Journal of Geophysical Research: Space Physics*, *121*, 1466–1482. https://doi.org/10.1002/2015JA021934

Sobral, J. H., Abdu, M. A., Zamlutti, C. J., & Batista, I. S. (1980). Association between plasma bubble irregularities and airglow disturbances over Brazilian low latitudes. *Geophysical Research Letters*, *7*, 980–982. https://doi.org/10.1029/GL007i011p00980

Stoneback, R. A., Heelis, R. A., Burrell, A. G., Coley, W. R., Fejer, B. G., & Pacheco, E. (2011). Observations of quiet time vertical ion drift in the equatorial ionosphere during the solar minimum period of 2009. *Journal of Geophysical Research*, *116*, A12327. https://doi.org/10.1029/2011JA016712

Su, Y.-J., Retterer, J. M., de La Beaujardiere, O., Burke, W. J., Roddy, P. A., Pfaff, R. F. Jr., et al. (2009). Assimilative modeling of equatorial plasma depletions observed by C/NOFS. *Geophysical Research Letters*, *36*, L00C02. https://doi.org/10.1029/2009GL038946

Sultan, P. J. (1996). Linear theory and modeling of the Rayleigh-Taylor instability leading to the occurrence of equatorial spread F. *Journal of Geophysical Research*, *101*(A12), 26,875–26,891. https://doi.org/10.1029/96JA00682

Woodman, R. F., & La Hoz, C. (1976). Radar observations of F region equatorial irregularities. *Journal of Geophysical Research*, *81*(31), 5447–5466. https://doi.org/10.1029/JA081i031p05447

Yizengaw, E., Retterer, J., Pacheco, E. E., Roddy, P., Groves, K., Caton, R., & Baki, P. (2013). Postmidnight bubbles and scintillations in the quiet-time June solstice. *Geophysical Research Letters*, *40*, 5592–5597. https://doi.org/10.1002/2013GL058307

Zhan, W., & Rodrigues, F. S. (2018). June solstice equatorial spread F in the American sector: A numerical assessment of linear stability aided by incoherent scatter radar measurements. *Journal of Geophysical Research: Space Physics*, *123*, 755–767. https://doi.org/10.1002/2017JA024969